# Chapter 12
# Fundamental Aspects
# of Electroless Copper Plating

## Perminder Bindra and James R. White

When an iron substrate is immersed in a solution of copper sulfate or silver nitrate, the iron dissolves while the copper or silver is plated out onto the surface of the substrate. This is called *immersion plating*. The process can be explained scientifically in terms of the electrochemical series, part of which has been reproduced in Table 12.1. The electrochemical series predicts the course of a reaction when two redox systems with different values for $E^0$, the standard redox potential, are brought into contact. The most electropositive redox system will be reduced (deposition), while the most electronegative will undergo oxidation (dissolution). Table 12.1 indicates that the standard redox potential for silver ($E^0$ = +0.799 V vs. SHE) or for copper ($E^0$ = +0.337 V vs. SHE) is more electropositive than that for iron ($E^0$ = -0.44 V vs. SHE). Therefore, the reactions occurring on the surface of the iron substrate are as follows:

*Anodic*
$$Fe^0 \rightarrow Fe^{2+} + 2e^- \qquad\qquad [1]$$

*Cathodic*
$$Cu^{2+} + 2e^- \rightarrow Cu^0 \qquad\qquad [2]$$

*or*
$$2Ag^+ + 2e^- \ 0 \rightarrow 2Ag^0 \qquad\qquad [3]$$

The surface of the metallic substrate consists of a mosaic of anodic and cathodic sites and the process will continue until almost the entire substrate is covered with copper. At this point, anodic oxidation virtually ceases; hence, plating is stopped. This imposes a limit on film thickness obtained by this technique, with average values of only 1 $\mu$m being observed. Other limitations of this method are that the coatings so produced usually lack adhesion and are porous in nature. The solution quickly becomes contaminated with ions of the base metal, and the process is only applicable to obtaining deposits of noble metals.

In order to overcome these limitations and to achieve thicker deposits, an alternative oxidation reaction is essential. This reaction must occur initially on a

**Table 12.1**
**Standard Redox Potential at 25° C**

| Reaction | Potential (V vs. SHE) |
|---|---|
| $Ag^+ + e^- \rightleftharpoons Ag^0$ | + 0.799 |
| $Cu^{2+} + e^- \rightleftharpoons Cu^+$ | + 0.158 |
| $Cu^{2+} + 2e^- \rightleftharpoons Cu^0$ | + 0.340 |
| $HCOOH + 2H^+ + 2e^- \rightleftharpoons HCHO + H_2O$ (pH = 0) | + 0.056 |
| $Ni^{2+} + 2e^- \rightleftharpoons Ni^0$ | + 0.230 |
| $Fe^{2+} + 2e^- \rightleftharpoons Fe^0$ | - 0.440 |
| $H_3PO_3 + 2H^+ + 2e^- \rightleftharpoons H_3PO_2 + H_2O$ (pH = 0) | - 0.500 |
| $HCOO^- + 2H_2 + 2e^- \rightleftharpoons HCHO + 3OH^-$ (pH = 14) | - 1.070 |
| $HPO_3^{2-} + 2H_2O + 2e^- \rightleftharpoons H_2PO_2^- + 3OH^-$ (pH = 14) | - 1.650 |

metallic substrate (activated substrate if the substrate is non-conducting) and subsequently on the deposit itself. From Table 12.1, it is clear that the redox potential for the reducing agent must be more negative than that for the metal being plated. The selection of the reducing agent is further limited in that the electrochemical reactions must only occur on the substrate, and not cause homogeneous reduction (decomposition) of the solution. An example of solution decomposition is the addition of formaldehyde ($E_R$ = +0.056 V vs. SHE at pH = 0) to silver nitrite solution, which causes spontaneous precipitation of metallic silver. A summary of common reducing agents that may be employed for electroless copper plating is given in Table 12.2. Theoretical conditions for the electroless plating of a metal may be determined from the Pourbaix (1) diagrams for the metal and the principal element in the reducing agent. Pourbaix diagrams show the ranges of potential and pH over which various ions, oxides, pure metals, etc., are thermodynamically stable. Potential-pH diagrams for the copper-water system and the carbon-water system are shown in Figs. 12.1 and 12.2, respectively. At potentials greater than +0.337 V vs. SHE, in acid solution, the copper ion is thermodynamically stable. For deposition of the metal to occur, the potential of the substrate must be lowered below this value, into the region where metallic copper is stable. In the carbon-water system, oxidation of formaldehyde to formic acid or formate anion occurs at potentials below +0.377 V vs. SHE over the entire range of pH. Thus the electrochemical processes that could theoretically occur on the metal surface in acid solutions are:

*Cathodic*
$Cu^{2+} + 2e^- \rightarrow Cu^0$   $E^0$ = +0.340                                    [4]

**Table 12.2**
**Components of Electroless Copper Plating Baths**

| Reducing agent | Complexant | Stabilizer | Exaltant |
|---|---|---|---|
| Formaldehyde | Sodium potassium tartrate (Rochelle salt) | Oxygen | Cyanide |
| Dimethylamine borane (DMAB) | Ethylenediamine tetraacetic acid (EDTA) | Thiourea | Proprionitrile |
| Sodium hypophosphite | Glycolic acid | 2-mercaptobenzo-thiazole | O-phenanthroline |
| | Triethanol amine | Diethyldithio-carbamate | |
| | | Vanadium pentoxide | |

*Anodic*

$$HCHO + H_2O \rightarrow HCOOH + 2H^+ + 2e^- \quad E^0 = +0.0564 \qquad [5]$$

When the two diagrams are superimposed, as shown in Fig. 12.3, the region of potential and pH over which plating is theoretically possible is indicated by the shaded region.

# COMPOSITION OF ELECTROLESS COPPER PLATING SOLUTIONS

Thermodynamic conditions for electroless copper plating are described in Fig. 12.3, but successful electroless plating cannot be guaranteed by simply adding a solution of the reducing agent to one containing metal ions. In actuality, local changes in pH can lead to precipitation of the metal in bulk solution. To overcome this difficulty, complexants are added to the plating bath to maintain the metal ion in solution. The complexants depress the free metal ion concentration to a value determined by the dissociation constant of the metal complex. In addition to preventing precipitation within the solution, the complexant also allows the bath to be operated at higher pH values. Figure 12.3 indicates that the thermodynamic driving force for copper deposition becomes greater as the pH increases.
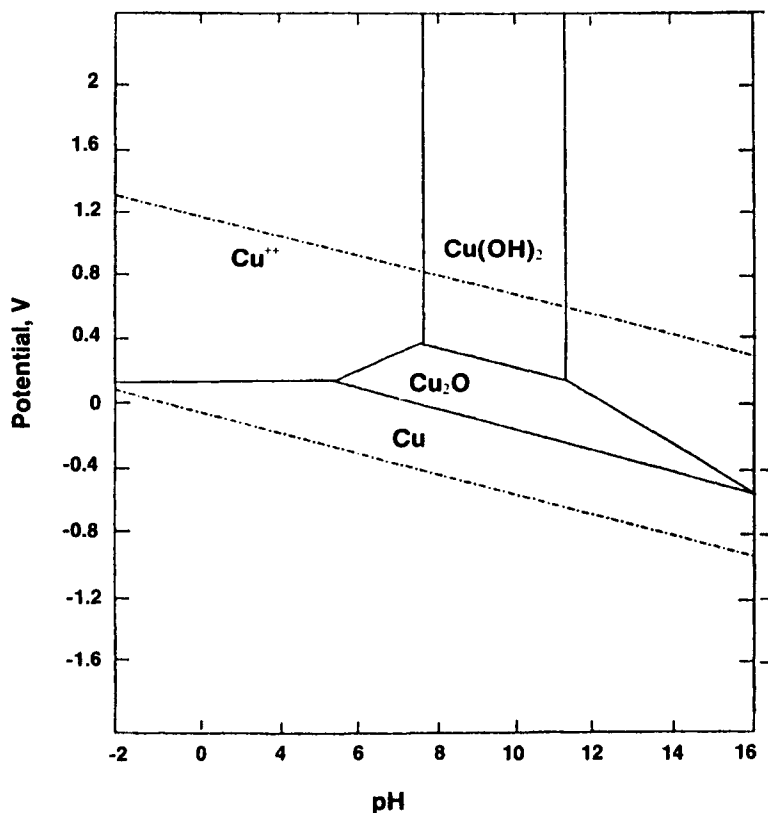
**Fig. 12.1—Potential-pH equilibrium diagram for copper-water system at 25° C. The area inside the dotted lines indicates the range of values within which various copper ions are thermodynamically stable.**

Table 12.1 shows that the redox potential for formaldehyde, $E_R$, at pH = 0 and pH = 14 differs by more than 1.0 V. Therefore, copper deposition is thermodynamically more favorable in alkaline solutions. However, copper precipitates at elevated pH values, and to prevent this from happening, a complexant such as sodium potassium tartrate is added to the plating formulation. Some common complexants used in commercial electroless copper processes are also listed in Table 12.2.

The selection and concentration of the complexant must be considered very carefully, because if the metal is too strongly complexed, insufficient free metal
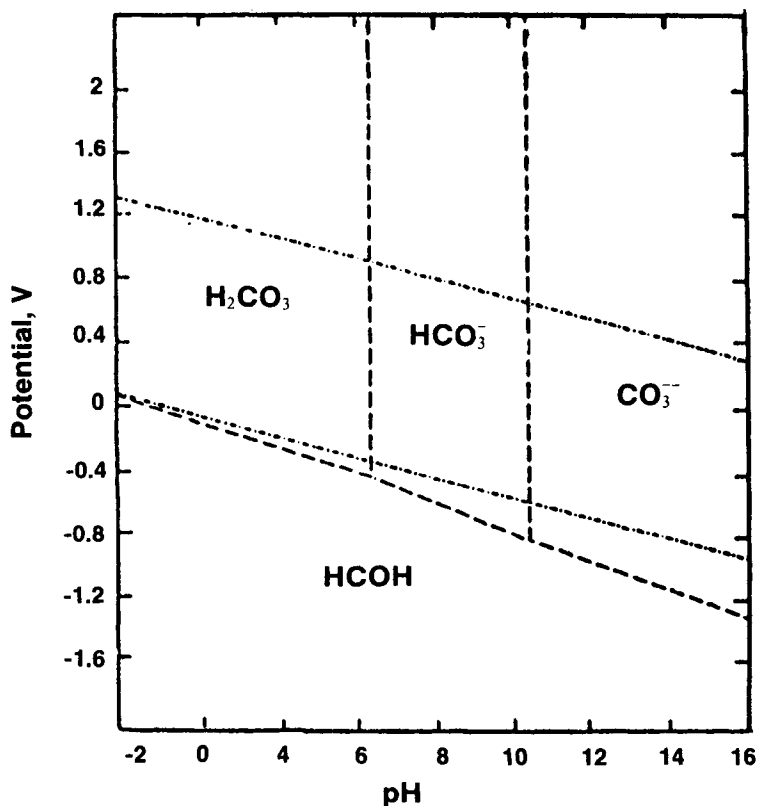
**Fig. 12.2—Potential-pH equilibrium diagram for carbon-water system at 25° C, showing the relative predominance of carbon in the form of methanol and carbonates.**

ions will be available for deposition. For instance, ethylenediaminetetraacetic acid (EDTA), which has a high stability constant, requires very careful control if plating is to occur.

Oxidation of the reducing agents employed in electroless copper plating invariably involves the formation of either hydrogen ($H^+$) or hydroxyl ($OH^-$) ions. Consequently, the pH of the plating solution changes during plating and thus affects the rate of deposition and the properties of the deposit. Therefore, buffers are added to stabilize the pH of the solution. These include carboxylic acids in acid media (which also act as complexants) and organic amines in alkaline solutions.
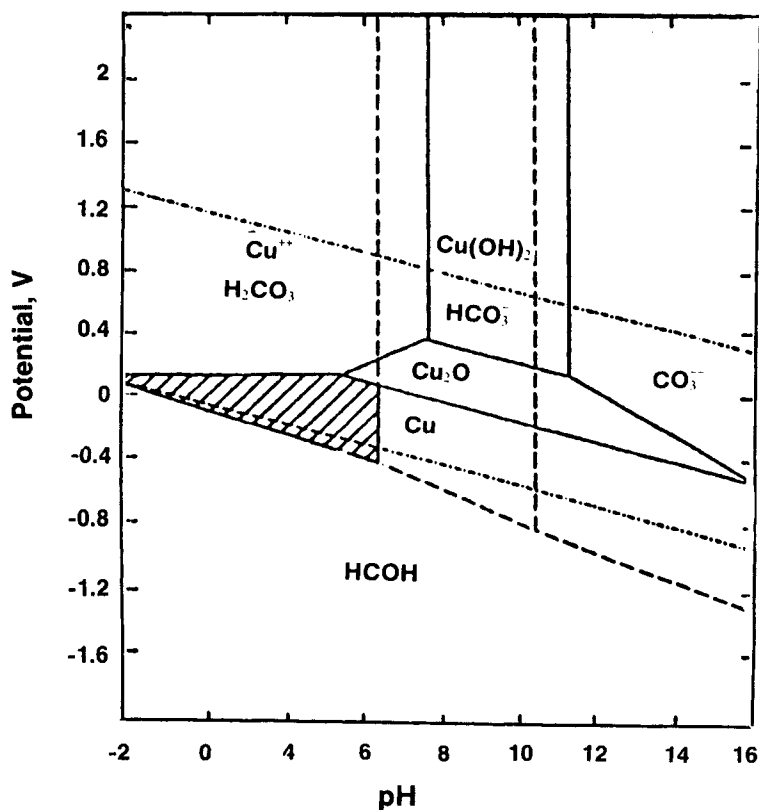
**Fig. 12.3**—Combined potential-pH diagram for copper-water and carbon-water systems, indicating the range of values within which metal deposition is possible.

Electroless plating formulations are inherently unstable and the presence of active nuclei such as dust or metallic particles can lead, over time, to homogeneous decomposition of the plating bath. The presence of the complexant in the correct concentration does not prevent this from occurring. To circumvent this problem, stabilizers such as 2-mercaptobenzothiazole are added to the bath in small concentrations. The stabilizers competitively adsorb on the active nuclei and shield them from the reducing agent in the plating solution. If, however, the stabilizers are used in excess, metal deposition may be completely prevented, even on the substrate itself.

The plating rate is sometimes inordinately lowered by the addition of complexants to the bath. Additives that increase the rate to an acceptable level without causing bath instability are termed *exaltants* or *accelerators*. These are generally anions, such as CN , which are thought to function by making the anodic oxidation process easier.

In summary, typical electroless plating formulations contain (a) a source of metal ions, (b) a reducing agent, (c) a complexant, (d) a buffer, (e) exaltants, and (f) stabilizers.

# THE MIXED POTENTIAL THEORY

The Wagner and Traud (2) theory of mixed potentials has been verified for several corrosion systems (3,4). According to this theory, the rate of a faradaic process is independent of other faradaic processes occurring at the electrode and depends only on the electrode potential. Hence, the polarization curves for independent anodic and cathodic processes may be added to predict the overall rates and potentials that exist when more than one reaction occurs simultaneously at an electrode. Wagner and Traud (2) demonstrated the dissolution of zinc amalgam to be dependent on the amalgam potential but independent of simultaneous hydrogen evolution processes.

The concept of mixed potentials can be explained by first considering a redox reaction of the type:

$$\text{Ox} + n\text{e} \underset{k_a}{\overset{k_c}{\rightleftharpoons}} \text{Red} \tag{6}$$

on an inert electrode. In Eq. 6, $k_c$ and $k_a$ are the rates for the cathodic and the anodic reactions, respectively. When equilibrium is established, the two opposing reactions occur at the same rate and no net current flows through the system. This condition may be expressed by the equation:

$$i_c = i_a = i^0 \tag{7}$$

where $i^0$ is the exchange current density and $i_c$ and $i_a$ are the cathodic and anodic current densities, respectively. The potential at which this equilibrium occurs is described as the equilibrium potential, $E^0$, and may be determined in the thermodynamic sense by the Nernst equation.

We next consider the case where two or more reactions occur simultaneously at the electrode surface (5,6). A copper/formaldehyde electroless plating process is a perfect example of such a case. The anodic reaction is the oxidation of the reducing agent (formaldehyde, methylene glycol, or hydrated formaldehyde in alkaline media):

$$2H_2C(OH)_2 + 2OH^- \rightarrow 2HCOOH + H_2 + 2H_2O + 2e^- \qquad [8]$$

$$(R^0 \rightarrow R^{z+} + Ze^-)$$
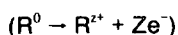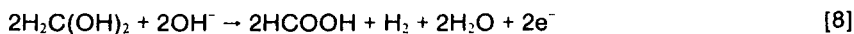
and the cathodic reaction is the reduction of the metal (copper) complex:

$$[CuL_6]^{(6n-2)-} \rightleftharpoons Cu^{2+} + 6L^{n-}$$
$$\downarrow \ 2e^- \qquad\qquad [9]$$
$$Cu^0$$

$$(M^{z+} + Ze^- \rightarrow M^0)$$

R and M denote the reductant and the metal, respectively.

The current potential curves for the anodic and the cathodic partial reactions in an electroless plating process are shown schematically in Fig. 12.4. It is clear from Fig. 12.4 that a necessary condition for electroless plating to occur is that
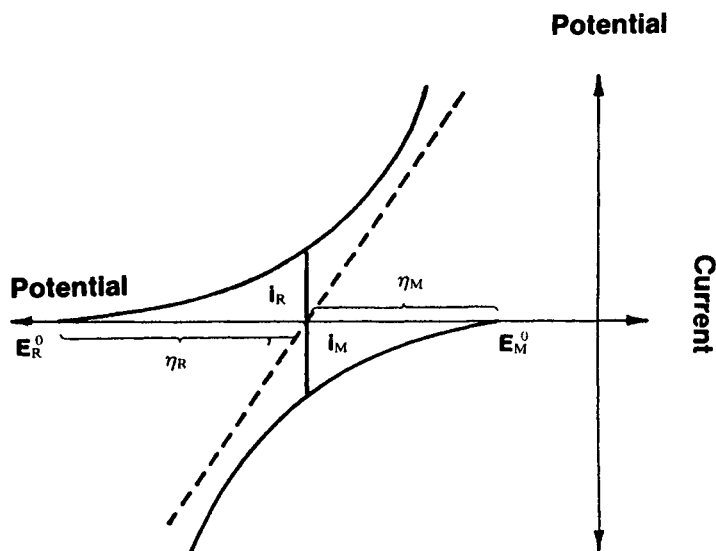


Fig. 12.4—Current-potential curves for the partial processes involved in electroless plating. Dotted line indicates the current-potential curve for the two simultaneous processes. $E_R^0$ and $E_M^0$ are equilibrium potentials.

the equilibrium potential for the reducing agent $E_R$ is more cathodic than the corresponding potential $E_M$ for the metal deposition reaction. At equilibrium, the Wagner-Traud postulate applies and the plating rate, $i_{plating}$, is given by:

$$i_{plating} = i_R = i_M \tag{10}$$

where $i_R$ and $i_M$ are the anodic and cathodic partial currents (with opposite signs). The potential associated with this dynamic equilibrium condition is referred to as the *mixed potential* $E_{MP}$. *The value of the mixed potential lies* between $E_R^0$ and $E_M^0$ and depends on parameters such as exchange current densities $i_R^0$ and $i_M^0$, Tafel slopes $b_R$ and $b_M$, temperature, and others. The mixed potential corresponds to two different overpotentials:

$$\eta_R = E_{MP} - E_R^0 \tag{11}$$

and

$$\eta_M = E_{MP} - E_M^0 \tag{12}$$

If the anodic and cathodic half cells are coupled (short-circuited), the measured current-potential curve is the algebraic sum of the partial current-potential curves for each electrode reaction, as shown in Fig. 12.4 by the dotted curve.

# APPLICATION OF THE MIXED POTENTIAL THEORY

In practice, the concept of mixed potentials is studied by constructing Evan's diagrams. In Fig. 12.5, a schematic Evan's diagram is constructed for the partial polarization curves shown in Fig. 12.4. The coordinates of intersection of the anodic and cathodic E vs. log i relationships give the value of the mixed potential $E_{MP}$ and the plating rate in terms of a current density $i_{dep}$. This suggests that the dynamic relationship between the mixed potential and the copper plating rate can be obtained from the individual electrode processes if their current-potential relationships are known. Such polarization curves have been obtained by one or more of the following methods: (a) by applying the steady state galvanostatic or potentiostatic pulse method to each partial reaction separately; (b) by applying potential scanning techniques to a rotating disk electrode; or (c) by measuring the plating rate from the substrate weight-gain as a function of the concentration of the reductant or the oxidant (8,9). The plating rate is then plotted against the mixed potential to obtain the Tafel parameter (7,8). These methods suffer from the usual limitations associated with the theory of mixed potentials. For example, extrapolation of the polarization curve for the catalytic decomposition of the reducing agent to the plating potential is not valid if the catalytic properties of the surface change with potential over the range of interest. It is also not valid if the rate determining step, and hence the Tafel slope,
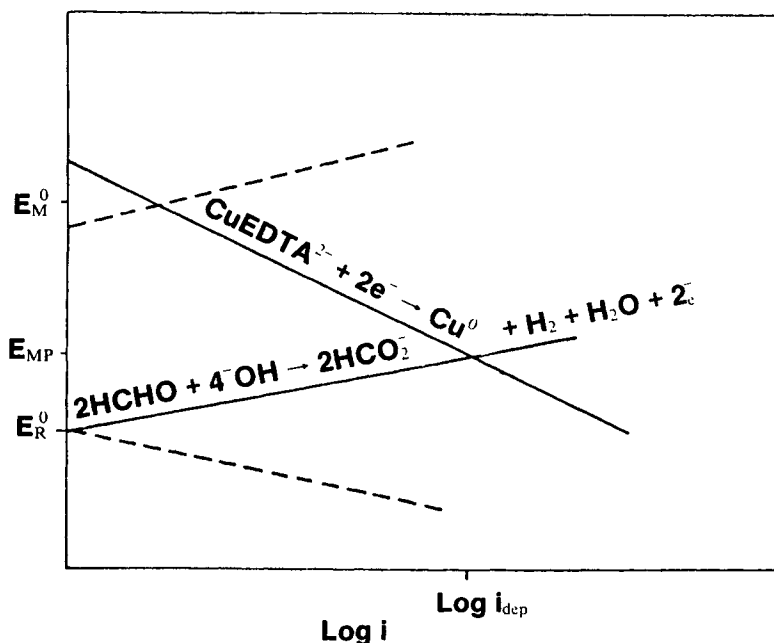
**Fig. 12.5—A schematic Evan's diagram showing the two partial processes of the additive copper bath.**

for any process changes in the potential range through which the polarization curve is extrapolated. Further, at least one of the two partial reactions involved in electroless metal plating is invariably diffusion-controlled. Therefore, the weight-gain method cannot be used to ascertain the plating mechanism unless the electrochemically-controlled partial reaction is first identified.

A further limitation to the extrapolation of polarization curves and to the application of the mixed potential concept to electroless plating, which is often not realized (10), is that the two partial processes are not independent of each other. For corrosion processes, such a limitation was first discovered by Andersen et al. (11). Bindra et al. (12) have found that same limitation to the application of the mixed potential theory to apply to electroless plating systems as well. These authors have developed a technique based on the mixed potential theory by which electroless plating processes may be classified according to

their overall mechanisms. For example, electroless plating of metals can involve a reaction that proceeds at a rate limited by diffusion. Donahue (13) has shown that the plating rate of copper (in a certain concentration range) in a copper-formaldehyde bath is determined by the rate of diffusion of copper ions to the plating surface. The technique described by Bindra et al. (12) allows a clear distinction between those reactions whose rate is controlled by the rate of diffusion of reactants to the plating surface, and those reactions whose rate is limited by some slow electrochemical step. The theory of this technique is described below.

In order to achieve conditions of controlled mass transfer, a rotating disk electrode (RDE) may be employed. The current resulting from the diffusion of metal ions to such a geometrical surface is expressed in Eq. 13 (14):

$$| i_M | = B_M' (C_M^\infty - C_M^s) \sqrt{\omega} \tag{13}$$

where $C_M^\infty$ is the bulk concentration of the reducing agent; $C_M^s$ the surface concentration, and $B_M'$ is a diffusion parameter (14,15).

$$B_M' = 0.62 \, n_M \, F \, D_M^{2/3} \, \nu^{-1/6} \, A \tag{14}$$

The symbols are defined in the appendix. For diffusion-controlled cathodic partial reactions, $C_M^s = 0$, and the limiting current $i_M^D$ is independent of potential and takes the form:

$$| i_M^D | = B_M' \, C_M^\infty \, \sqrt{\omega} \tag{15}$$

Similarly, the diffusion-limited current for the anodic partial reaction is:

$$i_R^D = B_R' \, C_R^\infty \, \sqrt{\omega} \tag{16}$$

The concentration of metal ions at the surface may be expressed by the Nernst equation:

$$E_M = E_M^0 + \frac{RT}{n_M F} \ln C_M^s \tag{17}$$

which, by substituting Eqs. 13 and 15, becomes:

$$E_M = E_M^0 + \frac{RT}{n_M F} \ln |(i_M^D - i_M)| - \frac{RT}{n_M F} \ln B_M' - \frac{RT}{n_M F} \ln \sqrt{\omega} \tag{18}$$

The corresponding equation for the reducing agent can also be worked out in a similar manner.

When the anodic partial reaction is under electrochemical control, the polarization curve is described by the equation:

$$E = E_R^0 - b_R \ln i_R^0 + b_R \ln i_R \qquad [19]$$

The anodic Tafel slope $b_R$ is given by:

$$b_R = \frac{RT}{(1 - \alpha_R)\, n_R F} \qquad [20]$$

Similarly, when the metal deposition reaction is activation controlled, the kinetics are described by the cathodic Tafel equation:

$$E = E_M^0 + b_M \ln |i_M^0| - b_M \ln |i_M| \qquad [21]$$

where:

$$b_M = \frac{RT}{\alpha_M\, n_M\, F} \qquad [22]$$

Since each partial reaction is either under electrochemical control or under mass transfer control, the overall reaction scheme consists of four possible combinations. These will be considered next, and the dependence of $E_{MP}$ on experimental parameters such as rotation rate $\omega$, and $C_R^\infty$ and $C_M^\infty$ determined.

*CASE 1: Cathodic partial reaction diffusion controlled—anodic partial reaction electrochemically controlled.*

The diffusion-limited cathodic partial current depends on $C_M^\infty$, $D_M$, and $\omega$, and its magnitude is given by Eq. 15. Then, combining Eq. 15 with Eq. 19, which describes the anodic partial reaction, by means of Eq. 10, gives:

$$E_{MP} = E_R^0 - b_R \ln i_R^0 + \frac{b_R}{2} \ln B_M'^2 \,\omega + b_R \ln C_M^\infty \qquad [23]$$

Equation 23 shows that the mixed potential is a linear function of $\ln \omega$ and $\ln C_M^\infty$ and that the Tafel slope for the anodic partial reaction may be obtained by plotting $E_{MP}$ against either of these experimental parameters. Similar functions have been obtained by Makrides (16) for corrosion processes. Case 1 is represented graphically in the symbolic diagram of Fig. 12.6.

Oxygen or air is frequently bubbled through electroless copper baths to oxidize any Cu(I) species formed, and thus avoid bath decomposition via Cu(I) disproportionation. Under these circumstances, there is another cathodic
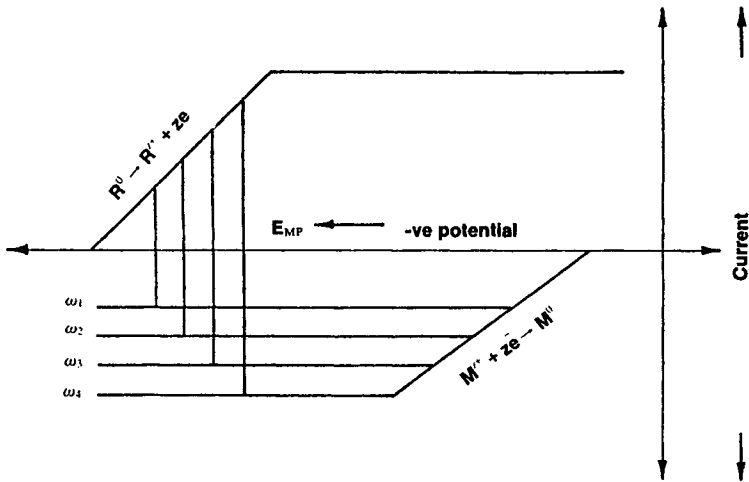
**Fig. 12.6—Symbolic representation of the overall reaction scheme for electroless metal deposition in which the cathodic partial reaction is diffusion-controlled and the anodic partial reaction is kinetically-controlled.**

current resulting from oxygen reduction, and the total cathodic current is the sum:

$$i_M' = i_M + i_{O_2} \tag{24}$$

where $i_{O_2}$ is the current for oxygen reduction. At the plating potential, $i_{O_2}$ is diffusion limited, that is, it is independent of the electrode potential, and therefore, is equivalent to a cathodic current applied externally.

Under these circumstances, Eq. 15 becomes:

$$|i_M^{D'}| = (B_M' C_M^\infty + B_{O_2}' C_0^\infty) \sqrt{\omega} \tag{25}$$

and Eq. 23 becomes:

$$E_{MP} = E_R^0 - b_R \ln i_R^0 + b_R \ln (B_M' C_M^\infty + B_{O_2}' C_{O_2}^\infty) + \frac{b_R}{2} \ln \omega \tag{26}$$

Therefore, the diagnostic criteria for Case 1 remains unchanged in the presence of oxygen in the plating bath.

*CASE 2: Cathodic partial reaction electrochemically controlled—anodic partial reaction diffusion controlled.*

This is the converse of Case 1, so that the anodic and cathodic partial reactions are described by Eq. 16 and Eq. 21, respectively. Combining them with the help of Eq. 10 yields:

$$E_{MP} = E_M^0 + b_M \ln | i_M^0 | - \frac{b_M}{2} \ln B_R^{\prime 2} \omega - b_M \ln C_R^{\times} \qquad [27]$$

Once again, $E_{MP}$ is linearly dependent on $\ln \omega$ and $\ln C_R^{\times}$.

The slope of $E_{MP}$ vs. $\ln$ plot is negative, thus making it easily distinguishable from Case 1. It can easily be shown that in the presence of oxygen in the plating solution, the form of Eq. 27 does not change.

*CASE 3: Both partial reactions electrochemically controlled.*

*CASE 4: Both partial reactions diffusion controlled.*

Such cases are rarely encountered in electroless plating baths. Therefore, detailed relationships between the mixed potential and other parameters are not worked out. Suffice it to say that in both cases, the mixed potential is independent of rotation rate.

# PARTIAL REACTIONS

A limitation to the application of the mixed potential theory to electroless plating is that the two partial reactions are not independent of each other. Such a limitation was alluded to as early as 1972 by Donahue (10), but *measurements* to clearly demonstrate the effect were not performed until much later (13). In an effort to demonstrate the interdependence of the partial reactions, Bindra et al. (12) performed kinetic and mechanistic measurements in the catholyte and the anolyte, as well as in the complete electroless copper bath separately. These measurements are discussed next.

## Cathodic Partial Reaction
The copper deposition reaction was studied with the help of a rotating disk electrode. Some typical results for the copper deposition partial reactions in the catholyte are shown in Figs. 12.7 through 12.9. The polarization curves obtained by applying the potential scanning technique at various rotation rates are displayed in Fig. 12.7. If the kinetics are first order with respect to copper ions in solutions, then the experimental disk currents are related to the rotation rate by the Levich equation, where all quantities are considered as positive (15):
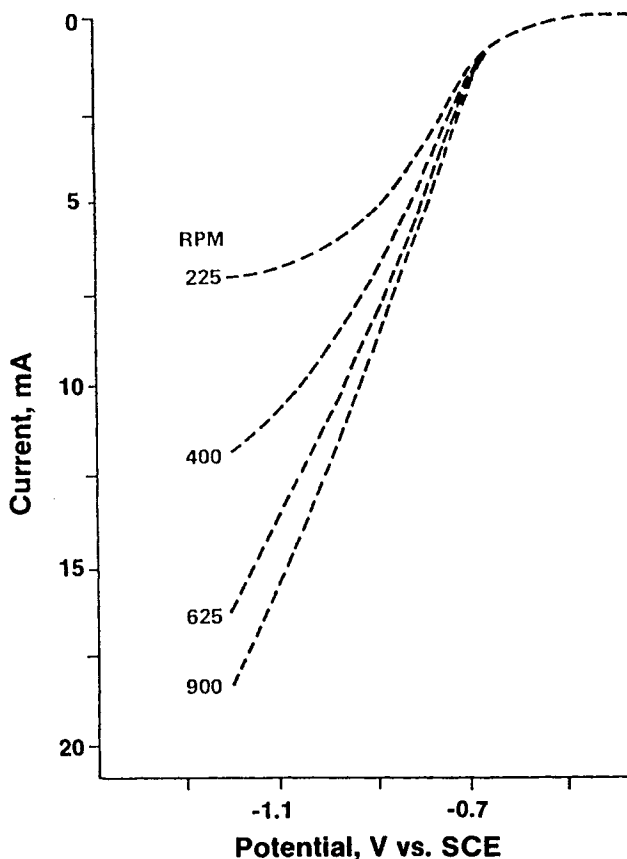
**Fig. 12.7—Rotating disk data for copper deposition in the catholyte at 70° C. Electrode area = 0.458 cm².**

$$\frac{1}{i_M} = \frac{1}{i_M^k} = \frac{1}{i_M^D} = \frac{1}{i_M^k} + \frac{1}{B_M\sqrt{\omega}} \qquad [28]$$

It is clear from Eq. 28 and Eq. 15 that $B_M = B'_M C_M^{\infty}$.

Figure 12.8 depicts plots of $1/i_M$ vs. $1/\sqrt{\omega}$ for the data shown in Fig. 12.7. These plots are linear and parallel, indicating that the copper deposition reaction is first
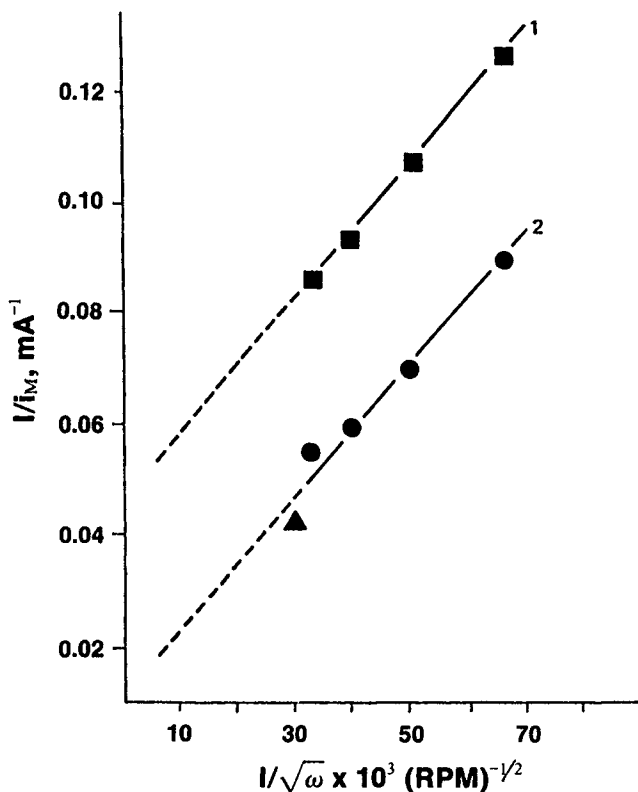
Fig. 12.8—Plots of $1/i_M$ vs. $1/\sqrt{\omega}$ for the rotating disk data from Fig. 12.7. (a) -0.8 V; (b) -0.95 V.

order in copper ion concentration. Figure 12.9 shows a mass transfer corrected Tafel plot at 70° C. There is a large linear region that yields a Tafel slope of -165 mV/decade. The value of the transfer coefficient, $\alpha_m$, calculated from this slope, comes close to 0.42. The polarization curve for copper deposition in the complete bath was also obtained and is shown in Fig. 12.10. This plot was obtained by the galvanostatic step method and yields a Tafel slope of -30 mV/decade.

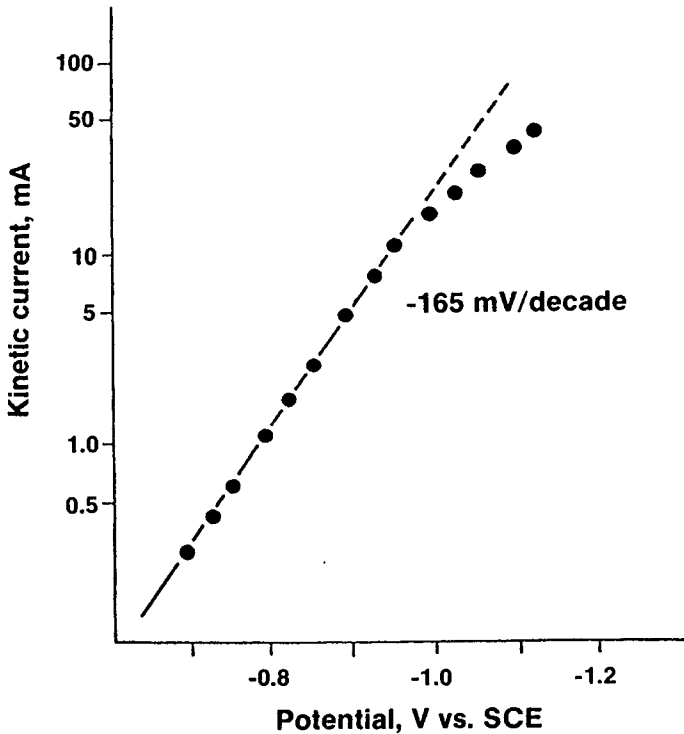A multistep, n-electron transfer metal deposition reaction may be written in the following form (17):

Fig. 12.9—Tafel plot for copper deposition in the catholyte at 400 rpm, 70° C, electrode area of 0.458 cm².

$$|E-E_M^0| = a - b_M \ln |i_M| \tag{29}$$

where $b_M$ is given by Eq. 22 and $\alpha_M$ is expressed as:

$$\alpha_M = (\gamma/v + n_M \beta_M) \tag{30}$$

In Eq. 30, $\gamma$ is the number of preceding steps prior to the rate determining step (rds), $v$ the stoichiometric number, and $\beta_M$ is the symmetry factor. The various pathways by which copper deposition in the catholyte may occur are as follows:
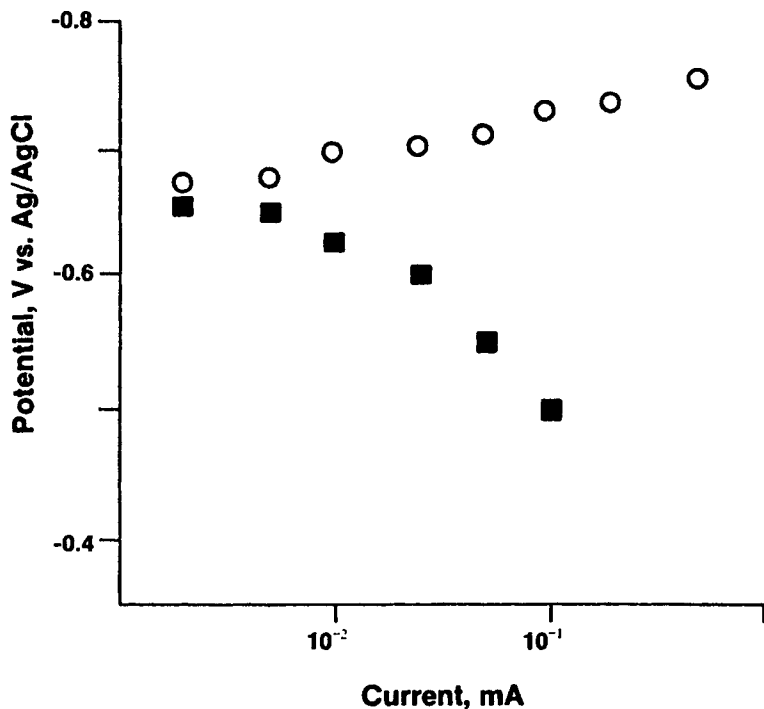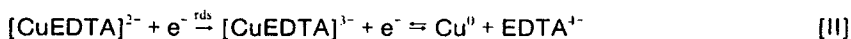
$$[CuEDTA]^{2-} + 2e^- \rightleftharpoons Cu^0 + EDTA^{4-} \tag{I}$$

**Fig. 12.10**—Polarization curves for copper deposition ( ○ ) and formaldehyde oxidation ( ■ ) obtained in the complete bath by the galvanostatic pulse method at 70° C and pH 11.7.
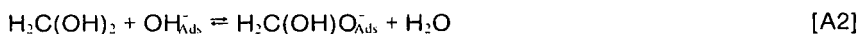
$$[CuEDTA]^{2-} + e^- \overset{rds}{\rightarrow} [CuEDTA]^{3-} + e^- \rightleftharpoons Cu^0 + EDTA^{4-} \qquad [II]$$

$$[CuEDTA]^{2-} + e^- \rightleftharpoons [CuEDTA]^{3-} \, e^- \overset{rds}{\rightarrow} Cu^0 + EDTA^{4-} \qquad [III]$$

One need only identify the values of r, v, $n_M$, and $\beta_M$ in order to determine the mechanism of copper deposition. Mechanism I is rejected on the grounds that a two electron transfer would require a very high activation energy. Besides, a $\beta_M$ value of 0.21 obtained from Eq. 30 for mechanism I is also unlikely. For mechanism III, Eq. 30 gives a $\beta_M$ value that is negative and therefore does not have a physical meaning. Hence, copper deposition in the catholyte occurs via

mechanism II, i.e., in two steps with the cupric-cuprous step as the rds. In the presence of cyanide ions in the catholyte, it is possible that the cuprous ion is stabilized by complexation with the cyanide. Such a mechanism was not investigated in this study. It is, however, interesting to note that the mechanism of copper deposition in the catholyte is similar to the mechanism postulated for copper deposition from $CuSO_4$ solutions.

## Anodic Partial Reaction

The oxidation of formaldehyde in the anolyte was investigated by the galvanostatic and the potentiostatic step methods (Figs. 12.10 and 12.11). Logarithmic analysis of the data gives linear plots of log i as a function of potential with Tafel slopes, which are considerably lower than those obtained in the complete electroless copper bath (Table 12.3). Such low Tafel slopes can only be interpreted in terms of a complex mechanism involving chemical and electrochemical steps. The proposed mechanism is shown in Reaction Scheme A.

*Scheme A*

$$HCHO + H_2O \rightleftharpoons H_2C(OH)_2 \qquad\qquad\qquad [A1]$$

$$H_2C(OH)_2 + OH^-_{Ads} \rightleftharpoons H_2C(OH)O^-_{Ads} + H_2O \qquad [A2]$$

$$H_2C(OH)O^-_{Ads} \rightleftharpoons HCOOH + \tfrac{1}{2}H_2 + e^- \qquad\qquad [A3]$$

$$HCOOH + OH^- \rightleftharpoons HCOO^- + H_2O \qquad\qquad [A4]$$

The observed Tafel slopes have a value around 110 mV/decade at 70° C (Table 12.3). Several reaction mechanisms could account for the experimentally observed kinetic parameters; three such mechanisms are described below:
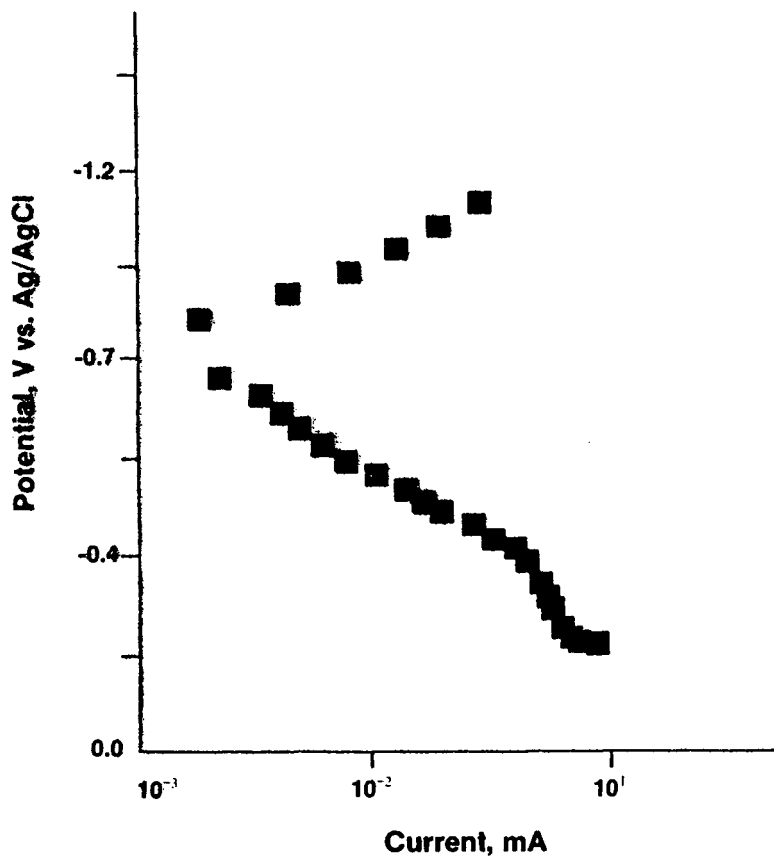
*Mechanism i*
Step A3 is rate-controlling, and the electron uptake is an inner sphere electron transfer, i.e., $(1 - \alpha_R)n_R = 1$. The Tafel slope expected (under conditions of Langmuir adsorption) if steps A2 and A4 are in quasi-equilibrium is then 70 mV/decade at 70° C.

*Mechanism ii*
Step A2 is the rds, but the electron transfer is outer sphere. In such a case, the Tafel slope expected under conditions of Langmuir adsorption has a value of 140 mV/decade at 70° C.

*Mechanism iii*
Step A2 is rate determining and A3 is in quasi-equilibrium. This is quite possible, since the formation of methylene glycolate anion, which is the electroactive species, is base catalyzed and therefore depends on pH value. A Tafel slope of 70

**Fig. 12.11—Polarization curve for formaldehyde oxidation and reduction obtained in the anolyte by the potentiostatic method at 70° C and pH 11.7.**

mV/decade at 70° C is expected in this case. However, the Tafel slope, and therefore the mechanism of formaldehyde oxidation would then be a function of formaldehyde concentration and pH. At pH equal to the pK value for step A2, this step is in quasi-equilibrium and mechanisms i or ii outlined above become operative.

It is clear that the observed Tafel slope of 110 mV/decade at 70° C cannot be accounted for by only one of the mechanisms outlined above. It is possible that

**Table 12.3
Analysis of Formaldehyde Oxidation Data:
Current Density vs. Potential**

| Method | Electrolyte | Slope, mV | Transfer coefficient |
|---|---|---|---|
| $dE_{MP}/d\log \omega$ | Complete bath | 104 | 0.34 |
| $dE_{MP}/d\log$ [HCHO] | Complete bath | 210 | 0.33 |
| $dE_{MP}/d\log$ [CuSO$_4$] | Complete bath | 188 | 0.37 |
| $dE_{MP}/d\log i_R$ (galvanostatic) | Complete bath | 185 | 0.38 |
| $dE_{MP}/d\log i_R$ (galvanostatic) | Anolyte | 110 | 0.64 |
| $dE_{MP}/d\log i_R$ (potentiostatic) | Anolyte | 115 | 0.61 |
| $dE_{MP}/d\log i_M$ (galvanostatic) | Complete bath | -30 ±5 | 0.43 |
| $dE/\log i_M$ (potential scanning) | Catholyte | -165 | 0.42 |

the components of the plating bath present in the anolyte (e.g., excess EDTA) affect formaldehyde decomposition and that the overall mechanism for this reaction is a combination of two or more mechanisms described above. In any case, it is clear that the mechanism of formaldehyde oxidation is more complex in the anolyte than in the complete plating bath, where it has been shown to be a catalytic process.

## Measurements in the Complete Copper Bath

The overall mechanism of copper plating was also determined by the application of the mixed potential theory to a rotating disk electrode. The mixed potential was observed as a function of rotation rate, $\omega$, of the RDE and the bulk concentrations $C_M^x$ of metal ions. The data obtained is shown in Figs. 12.12 and 12.13. It is clear that each one of these plots is a straight line. Using the criteria developed earlier, it is relatively simple to assign a mechanism to the electroless plating process. We first note that the mixed potential increases with both rotation rate $\omega$ and the concentration, $C_M^x$, of metal ions in the plating bath; that is, the slopes for the plots in Figs. 12.12 and 12.13 are positive. This behavior is indicative of diffusion-controlled copper deposition partial reactions and activation-controlled formaldehyde decomposition reactions. The same mechanism with respect to the copper deposition partial reaction has been noted previously by Donahue (13).

Verification of the theory developed for this technique is obtained by comparing the measured slope of the rotation rate dependence, $dE_{MP}/d\ln \omega$, with
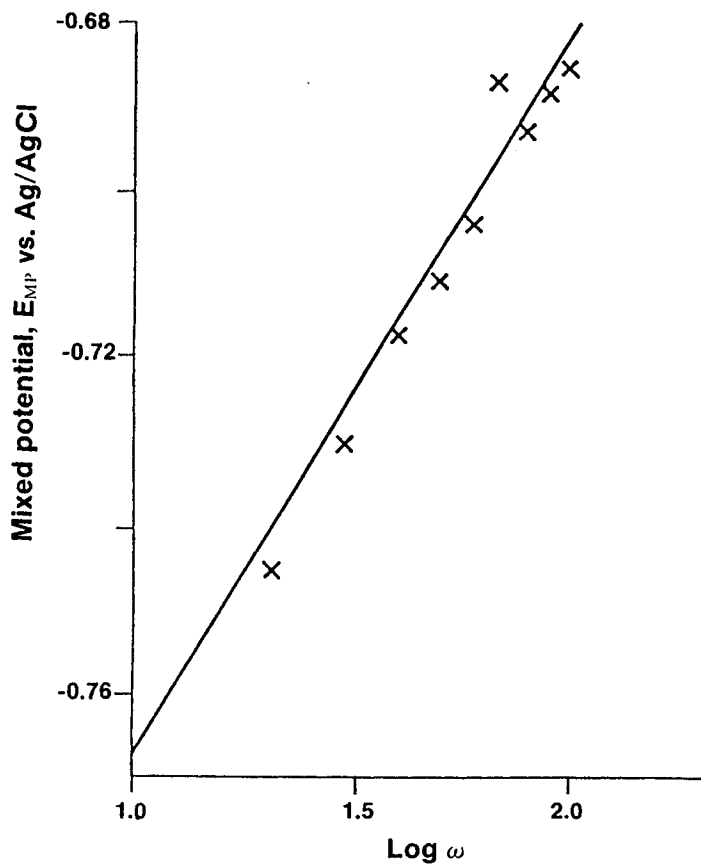
**Fig. 12.12**—Plot of the mixed potential of the plating solution as a function of rotation rate. Temperature = 70° C, pH = 11.7.

the concentration dependence $dE_{MP}/dlnC_M^x$. These slopes are reported in Table 12.3, which shows that:

$$\frac{dE_{MP}}{dlnC_M^x} = 2 \times \frac{dE_{MP}}{dln\omega} = b_r \tag{31}$$

This result is predicted by Eq. 23. Clearly, this simple technique is capable of measuring *in situ* the Tafel slope for either the anodic partial reaction or the
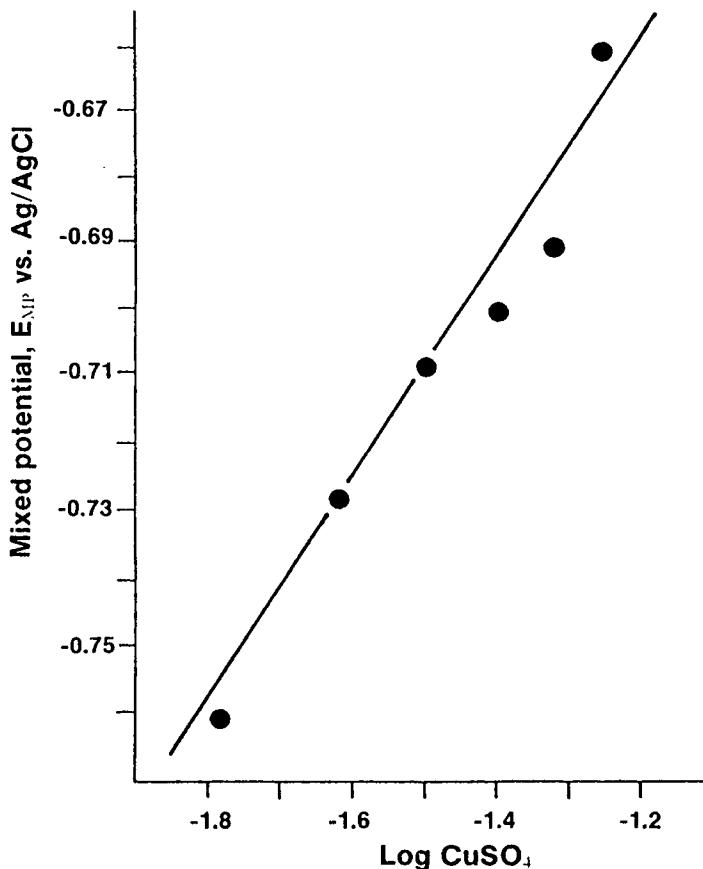
**Fig. 12.13—Plot of the mixed potential of the plating solution vs. the logarithm of the CuSO₄ concentration. Temperature = 70° C, pH = 11.7.**

cathodic partial reaction, depending on the overall mechanism of the plating process. In the electroless copper bath under study in this investigation, $b_r$ is the Tafel slope for formaldehyde oxidation and has the value $\sim+210$ mV/decade at 70° C. In order to further substantiate the validity of this approach, galvanostatic step measurements were also performed in the electroless copper bath. The Tafel plot obtained is shown in Fig. 12.14. The Tafel slope obtained has the value of +185 mV/decade at 70° C, which is in reasonable agreement with the value obtained by the technique based on observation of the behavior of the mixed
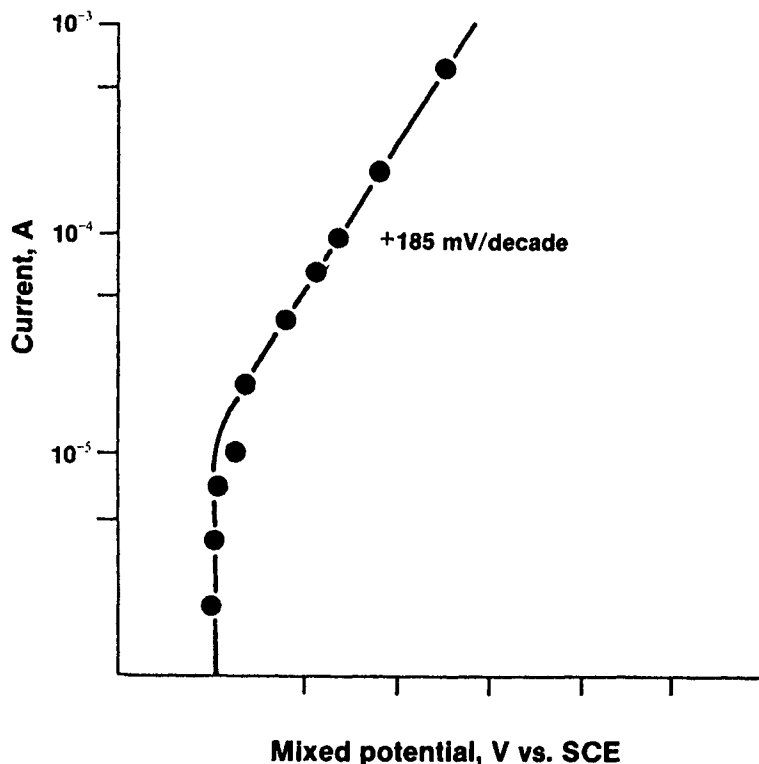
**Mixed potential, V vs. SCE**

Fig. 12.14—Polarization curve for formaldehyde oxidation obtained in the complete bath by the galvanostatic pulse method at 70° C and pH 11.7.

potential. This latter technique is therefore important, not only from the point of view of ascertaining the overall mechanism of electroless metal plating, but also as a convenient method of determining the Tafel slope for the partial reaction under electrochemical control.

Tafel slopes in the range of 185 to 210 mV/decade correspond to values of the anodic transfer coefficient, $(1 - \alpha_R)n_R$, which are substantially lower than 0.5 (Table 12.3, column 4). The observed value of the transfer coefficient is known to deviate from 0.5 when the actual electron transfer occurs across only a fraction of the Helmholtz double layer, i.e., when the reacting species are specifically adsorbed and the electron transfer occurs in the inner Helmholtz plane. Such behavior is characteristic of catalytic reactions. The large value of the Tafel slope implies control by the first electron transfer under Temkin adsorption conditions.

Under the circumstances, the oxidation of formaldehyde in electroless copper plating may be described by scheme A.

Formaldehyde in aqueous solutions exists predominantly in the electro-inactive hydrated form. Reaction A1 above represents the quasi-equilibrium of the hydration reaction at high pH values. The anion of the hydrated form, which is the electroactive species, can then be created either in the bulk solution by a general base catalysis (18) or be generated on the substrate surface by interaction with adsorbed OH , as shown in Reaction A2. The high value of the Tafel slope indicates a catalytic reaction, and therefore supports the participation of the substrate surface, either as an antecedent step to the electron uptake or as a proceeding step to stabilize reaction intermediates (19,20). Measurements performed here do not allow a distinction as to whether the hydrogen abstraction in Reaction A4 precedes the electron uptake or follows it. Nonetheless, Reaction A3 is the rds in the overall mechanism. The overall stoichiometry of the reaction is in agreement with that proposed by Lukes (21).

Further support for the validity of the mixed potential technique can be found in the Tafel curve for the copper deposition partial reaction obtained in the complete bath (Fig. 12.10). The Tafel slope observed in this case has a value of -30 ±5 mV/decade. For pure diffusion control by metal ions in the plating bath, the Tafel equation may be expressed as (19):

$$|E - E_M^0| = \frac{RT}{2F} \ln \left[ 1 - \left( \frac{i_M}{i_M^D} \right) \right] \qquad [32]$$

At potential values where $i_M \ll i_M^D$, Eq. 32 reduces to the usual form of the Tafel equation:

$$|E - E_M^0| = \alpha' - \frac{RT}{2F} \ln |i_M| \qquad [33]$$

where the term $\alpha'$ is different from the term $\alpha$ in the Tafel equation (cf. Eq. 29). Equation 33 exhibits a Tafel slope of -37 mV/decade at 70° C, suggesting that the cathodic partial reaction in the electroless copper process is diffusion controlled.

There are two possible mechanisms by which this could occur. These are (1) rate-controlling diffusion of $[CuEDTA]^{2-}$ to the substrate, followed by dissociation of the complex prior to reduction; and (2) dissociation of the $[CuEDTA]^{2-}$ complex in the bulk solution, followed by rate-controlling diffusion of aqueous copper ions to the substrate for reduction. The techniques used in this investigation do not allow a distinction between these two mechanisms. In either case, the rate of reduction of copper ions is much faster than the rate at which electrons are released by the reducing agent. The fact that the cathodic partial reaction in electroless copper plating is diffusion-controlled is in total

agreement with the overall mechanism for electroless copper plating ascertained by observing the behavior of the mixed potential as a function of $\omega$ and $C_M^x$.

### Interdependence of the Partial Reaction

To establish the interdependence or otherwise of the partial reactions in electroless copper plating, Tafel slopes for the partial reactions were obtained in the complete plating bath, as well as in the catholyte and anolyte separately. The Tafel slope for the copper deposition reaction (Table 12.3) in the catholyte indicates a stepwise reaction mechanism, with the cupric-cuprous step as the rds. In the electroless plating bath, the Tafel slope for the cathodic partial reaction has a value of -30 $\pm$5 mV/decade, indicating diffusion control for this reaction. The difference in mechanisms in the catholyte and in the plating bath is attributed to the presence of the reducing agent and the anodic partial reaction in the bath. Electroless plating processes occur via two consecutive reactions: Electrons are released during the partial anodic reaction and are consumed by the cathodic partial reaction, which also happens to be the metal deposition reaction. The overall rate of the electroless plating process is therefore governed by the slower of the two partial reactions. In the bath formulation studied in this investigation, the exchange current density for the formaldehyde oxidation at $E_{MP}$ is at least two orders of magnitude lower than the exchange current density for the copper deposition reaction. Therefore, whatever the mechanism of copper deposition in the catholyte, the electroless plating process is controlled by the kinetics of the formaldehyde oxidation reaction, i.e., the rate of the copper deposition partial reaction is totally dependent on the kinetics of the anodic partial reaction. Hence the two partial reactions in electroless copper plating are not independent of each other.

Further evidence in support of this theory is provided by the Tafel plots for formaldehyde oxidation in the plating bath and in the anolyte (Table 12.3). There is considerable difference in Tafel slopes in the two solutions, indicating a difference in the mechanism of the reaction in the two environments. Clearly, the anodic partial reaction in the electroless plating bath is affected by the presence of copper ions in the bath.

# KINETICS OF ELECTROLESS COPPER DEPOSITION

A number of studies have emerged regarding the kinetics of electroless copper deposition (6,8,22-24). Most have analyzed results in terms of classical kinetic theory and utilize the following rate equation:

$$r = k[Cu^{2+}]^a \, [OH^-]^b \, [HCHO]^c \, [LIGAND]^d \qquad\qquad [34]$$

A summary of reaction orders, for various components, is shown in Table 12.4. The diversity of reaction orders, and in some cases negative reaction orders, is attributable to a number of factors. First, different substrates are employed that

## Table 12.4
## Summary of Reaction Orders
## For Electroless Copper Baths

| Cu | OH | HCHO | Ligand | Reference |
|------|--------|------|------------------|-----------|
| 0.47 | 0.18 | 0.07 | - (tartrate) | 56 |
| 0.37 | 0.25 | 0.08 | 0.19 (tartrate) | 6 |
| 0.78 | <0.02 | 0.13 | <0.02 (tartrate) | 8 |
| 0.43 | -0.70 | 0.16 | -0.04 (EDTA) | 22 |
| 1.00 | 0.37 | 0.00 | - (EDTA) | 23' |
| 0.00 | 1.00 | 0.68 | - (EDTA) | 23ᵇ |
| 0.00 | 0.00 | 1.00 | 0 (EDTA) | 5 |

'Final deposition rate.
ᵇInitial deposition rate.

have varying degrees of catalytic activity. In some cases metal substrates are used, while catalyzed dielectrics are used in others. Second, the time frame of the measurement is critical since the rate has been observed to decrease with time (6,23). The initial rate (at copper coverages less than 25 $\mu$g Cu/cm$^2$) is generally larger than the subsequent steady state rate.

A third factor is associated with mass transfer effects. The importance of understanding how interfacial (surface) concentrations differ from bulk concentrations has been stressed (13). In general, the interfacial concentration of a species C is given by the following equation:

$$C = C_b + 10^3 \, N \, \delta/D \qquad [35]$$

where $C_b$ is the bulk concentration, N is the flux of species C to the electrode surface, $\delta$ is diffusion layer thickness, and D is the diffusion coefficient for C.

For electroless plating baths, in the absence of forced convection, the primary means of mass transfer results from microconvection by hydrogen bubbles. Estimates for values of C, under this condition, have been given by Donahue (13).

Finally, most practical systems contain additional components to enhance metallurgy or stabilize the bath. These components certainly impact the kinetics of the system but render the system too complex for study. Thus, more studies are based only on the four primary constituents of the plating bath.

A variety of measurement techniques have been utilized to obtain kinetic data. Most investigators utilize some form of the mixed potential theory described in

the previous section and correlate results to the weight gain observed at the cathode. A method based on a resistance probe has been described in which the cathode comprises one arm of a wheatstone bridge (25). The plating rate may be monitored by observing changes in resistance with time.

Dumesic et al. described an optical technique based on the absorption of monochromatic light at a sensitized transparent rotating cylinder (23). With this method they were able to clearly distinguish between changes in the initial rate and the final rate region. For example, the reaction order for formaldehyde changed from 0.68 during the initial stages of deposition to 0 during the final stage.

A method based on weight gain has been reported that utilizes a quartz microbalance (24). The advantage of this technique, compared to macroscopic weight measurements, is that the microbalance is an *in situ* technique.

The effect of cupric ion on the kinetics varies with concentration and is attributable to mass transfer effects (13). At low bulk cupric ion concentrations (i.e., less than 0.01M), the interfacial concentration (Eq. 35) is low and mass transfer plays a decisive role. For intermediate values of $Cu_b^{2+}$ (i.e., $0.01M < Cu_b^{2+} < 0.2M$), the interfacial concentration falls in an intermediate range between 20 and 80 percent of the bulk concentration. Thus, the system is under mixed kinetic and mass transfer control. At higher concentrations the effect is primarily kinetic. Dumesic points out that during the initial stage of the reaction, the rate is independent of cupric ion concentration, assuming no mass transfer limitation (23).

The influence of formaldehyde concentration is generally small during steady state (final) deposition, i.e., reaction orders less than 0.1 have been reported. However, during initial stages the reaction was found to be first order with respect to formaldehyde.

The effect of hydroxide ion concentration is similar to that reported for formaldehyde. During steady state deposition the influence is minimal, but during initial stages the influence is greater. A maxima in the plating rate, as a function of pH, was reported by Schoenberg (26). This is attributable to competition between hydroxide ion and methylene glycolate for copper coordination.

Donahue examined a large number of plating bath compositions, based on mixed potential analysis, and obtained the following empirical rate equation (22):

$$r = 2.81 \frac{[Cu^{2+}]^{0.43} [HCHO]^{0.16}}{[OH^-]^{0.70} [EDTA]^{0.04}} \exp. \quad 11.5 \frac{T-313}{T} \qquad [36]$$

The correlation coefficients for formaldehyde and EDTA were low, although 90 percent of the measured plating rates were within 20 percent of the predicted values.

A more recent study is based on the following Arrhenius equation (24):

$$r = A \exp [-\Delta E^{\ddagger}/RT]C_{MG^-} \tag{37}$$

The experimental conditions were such that the reaction was first order with respect to formaldehyde (actually methylene glycolate $MG^-$) and zero order for all other components. An activation energy of 60.9 kJ/mole was obtained. The proposed rds is the cleavage of the carbon hydrogen bond of methylene glycolate. Isotopic substitution of $CD_2O$ for $CH_2O$ resulted in a primary isotope effect of $kH/kD = 5$.

# CATALYSTS FOR ELECTROLESS COPPER PLATING

The rate determining step for the electroless copper bath is most frequently associated with the anodic process, which is generally under kinetic control. In order to evaluate the catalytic activity of various metals, the oxidation of common reductants may be studied by electrochemical techniques. Ohno et al. have investigated the polarization behavior of a number of reductants on a variety of solid electrodes and determined that copper is most catalytically active for formaldehyde oxidation, as compared to other common reductants (27). Their results are shown in Fig. 12.15.* The potentials for each metal substrate are those observed when the electrodes were subject to a constant current of $10^{-4}$ A/cm$^2$. $E_r$ is the standard reduction potential for each reductant. To achieve relatively thick electroless copper deposits, the plating reaction must be autocatalytic with respect to copper, and therefore, most commercially available electroless copper baths are formaldehyde-based.

The electrolcatalytic activity of various metals for formaldehyde oxidation has been evaluated by a number of workers, primarily by cyclic voltammetry (Fig. 12.16). Bindra et al. determined that palladium and platinum were among the best catalysts in alkaline media (28). Results were expressed in terms of a volcano plot (Fig. 12.17), which compares the normalized peak current for formaldehyde oxidation to the enthalpy of formation of the metal formate. The metal formate is a proposed intermediate in the formaldehyde oxidation pathway. Enyo evaluated several metals at more negative potentials (i.e., closer to the onset of the electrocatalytic oxidation) and concluded that Au was a better catalyst than Pd or Pt in alkaline media (Fig. 12.18) (29).

In acid media, Au has very low catalytic activity compared to Pt and Pd. This is attributed to the importance of the surface oxide structure in catalyzing the electrooxidation reaction. For Pt and Pd, the onset of formaldehyde oxidation occurs near the onset of surface oxide formation (Fig. 12.16). Since oxide formation occurs at more positive potentials on Au, compared to Pd or Pt,
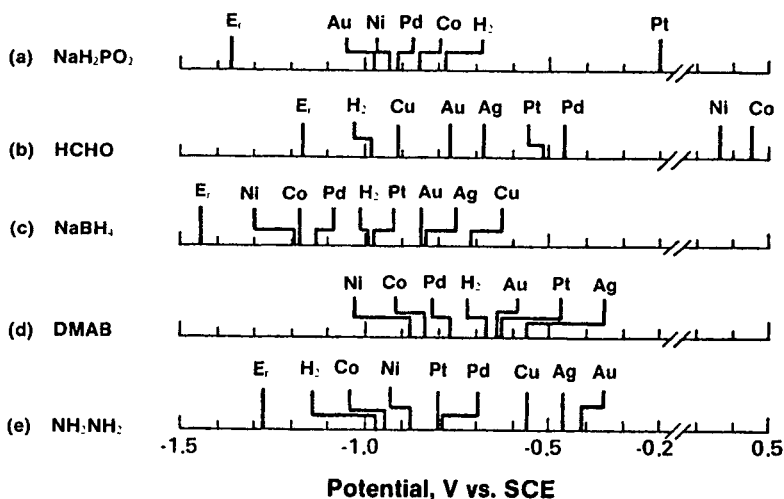
Fig. 12.15—Catalytic activities of metals (the potentials at $10^{-1}$ A/cm$^2$) for anodic oxidation of different reductants. $E_R$ = oxidation-reduction potentials of reductants. $H_2$ = reversible hydrogen potentials. Conditions: (a) 0.2M NaH$_2$PO$_2$ + 0.2M Na-citrate + 0.5M H$_3$BO$_3$, pH 9.0, 343 K; (b) 0.1M HCHO + 0.175M EDTA·2Na, pH 12.5, 298 K; (c) 0.03M NaBH$_4$ + 0.175M EDTA·2Na, pH 12.5, 298 K; (d) 2.0 g/dm$^3$ DMAB + 0.2M Na-citrate = 0.5M H$_3$BO$_3$, pH 7.0, 298 K; (e) 1.0M N$_2$H$_4$ + 0.175M EDTA·2Na, pH 12.0, 298 K.

formaldehyde oxidation is correspondingly shifted to more positive potentials. However, in alkaline media the role of the surface oxides is less predominant since oxygen atoms for the reaction may be supplied by solution species, e.g., OH$^-$. Therefore, Au is a far better catalyst in alkaline media than in acid media.

Alloys have been examined for their catalytic activity for formaldehyde oxidation and in many cases show enhanced activity when compared to constituent metals. Enyo showed that Pd and Au alloys were more active catalytically than Pd (Fig. 12.18) (29). The activity increased montonically with increasing Au content. Similarly, Au and Pt alloys were determined to be more active than Pt (30). It has also been demonstrated that Cu and Ni alloys are more active for formaldehyde oxidation than Cu (31). The composition Cu$_{89}$Ni$_{11}$ had the highest activity and decreased with increasing Ni content. This observation has a further consequence, since the inclusion of small quantities of Ni$^{2+}$ in a copper plating bath results in alteration of the physical properties of the deposit, attributable to inclusion of nickel in the deposit. Therefore, it is possible to
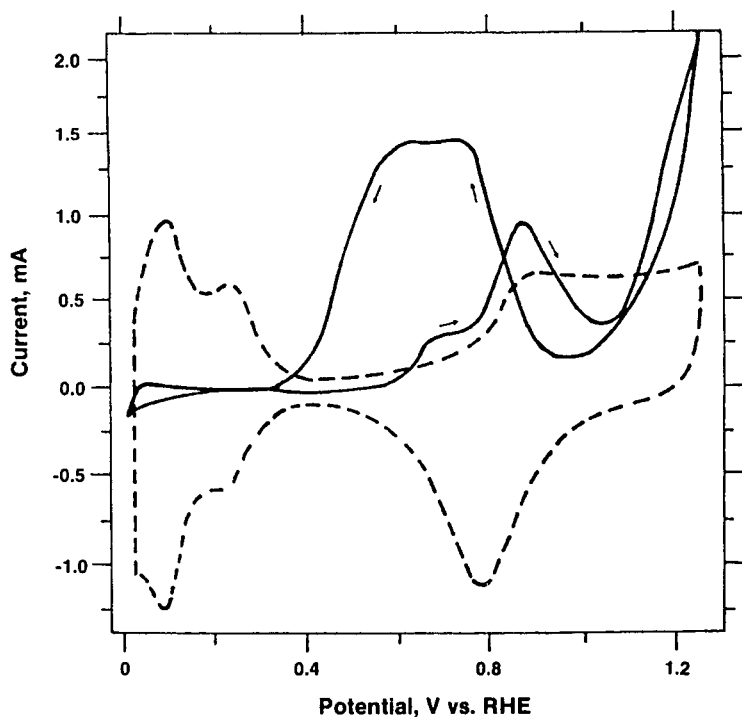
**Fig. 12.16—Cyclic voltammetry curves for Pt in 1M HClO₄ (dashed curve, scale on right) and 1M HClO₄ + 0.1M HCHO (solid curve). Ar saturated, electrode area = 0.458 cm², scan rate = 0.1 V/sec, temperature = 25° C.**

enhance both deposit metallurgy and catalytic activity by judicious inclusion of foreign metals in the bath.

The mechanism for formaldehyde oxidation is dependent on the nature of the catalytic substrate. In some cases (e.g., group VIII metals), the reaction is not accompanied by hydrogen generation and proceeds as follows (28):

$$H_2C(OH)O^- + 2OH^- \rightarrow 2HCO_2^- + 2H_2O + 2e^- \tag{38}$$
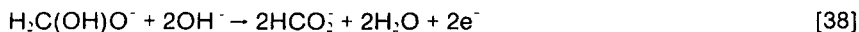
However, for group 1B metals, the reaction is accompanied by hydrogen production, as shown in Eq. 39:

$$2H_2C(OH)O^- + 2OH^- \rightarrow 2HCO_2^- + 2H_2O + H_2 \uparrow + 2e^- \tag{39}$$
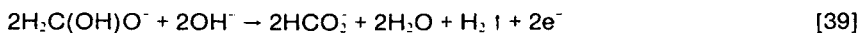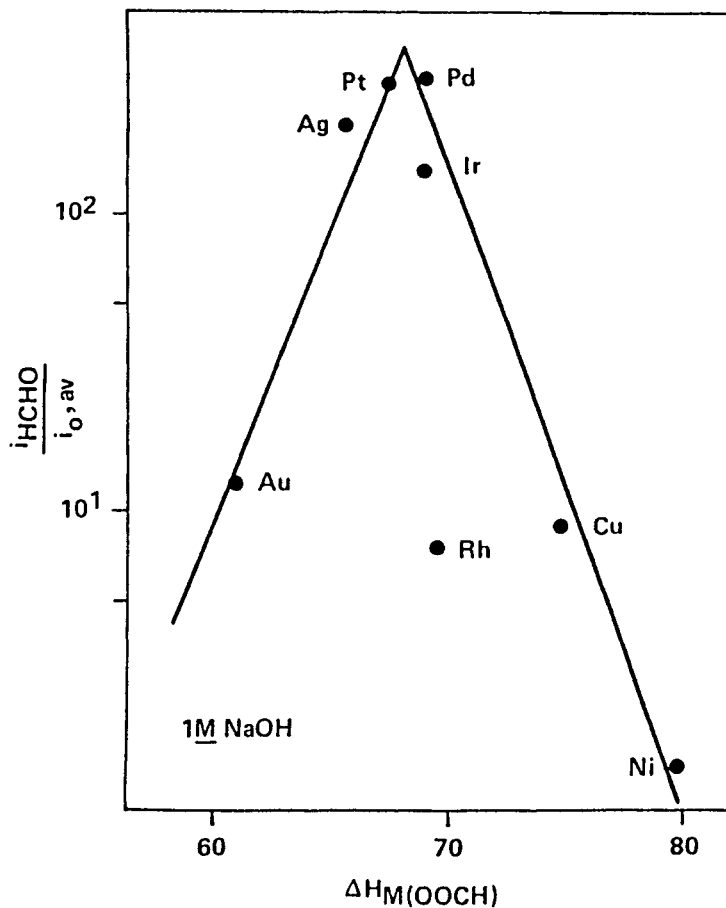
Fig. 12.17—Plot of HCHO oxidation currents in 1M NaOH vs. enthalpy of formation of metal formate.

This may be explained by the disposition of the intermediate metal hydride (adsorbed hydrogen radical). The hydrogen radical, when adsorbed on Pt, is oxidized at potentials where formaldehyde oxidation occurs. Therefore, radical recombination to form hydrogen gas is unfavorable. In contrast, on copper, recombination of hydrogen radicals does occur and hydrogen gas evolution is
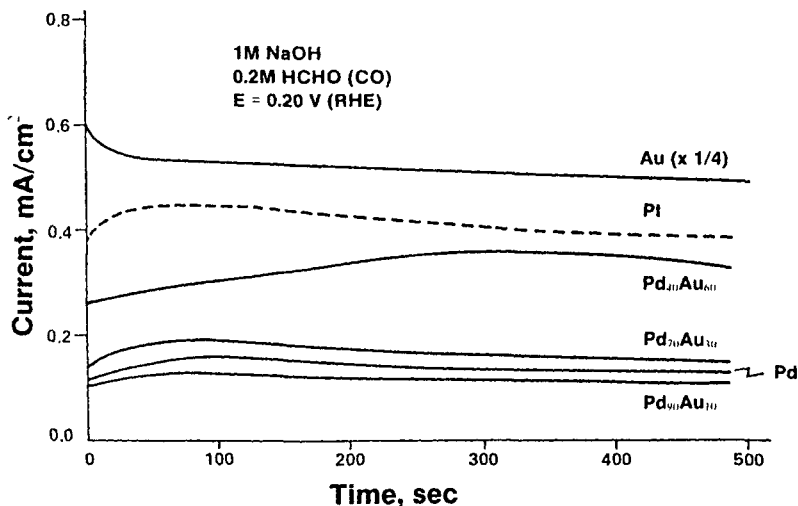
**Fig. 12.18**—Time dependence of the currents of electrooxidation of 0.2M HCHO in 1M NaOH solution at 30° C. Curve for Au is shown in ¼ times reduced scale.

observed. Oxidation of the hydrogen radical is kinetically unfavorable at the potentials where formaldehyde oxidation is observed.

In practice, the most commonly utilized catalysts are comprised of Pd and Sn. A two step catalysis (seeding) process has been described where a non-catalytic surface is first treated by immersion in an acidic solution of $SnCl_2$, followed by immersion in an acidic solution of $PdCl_2$ (32). Stannous is thermodynamically capable of reducing Pd. The resultant reduced Pd is an active catalyst for formaldehyde oxidation.

Single step Pd and Sn catalysts have also been described whereby a colloid consisting of Pd and Sn is formed by digestion of an acidic $PdCl_2$ and $SnCl_2$ mixture (33-35). Such catalysts are the most widely used in practice. In the early stages of digestion, a complex is formed with a Pd:Sn ratio of 1:3 (36,37). As digestion proceeds, a colloid is formed and is comprised of a reduced Pd metal nucleus. The reaction proceeds according to Eq. 3, where $(Pd-Sn)_x$ denotes the complex.

$$(Pd-Sn)_x \rightarrow Pd^{II} + Sn^{4+} + 2Sn^{2+} \qquad [40]$$

The colloid is stabilized by a shroud of $SnCl_3^-$ ions imparting a negative charge to the particle. At least three species of tin have been identified by Mossbauer

spectroscopy and include stannic and two stannous components (36,37). The two stannous components are identified as part of the Pd-rich core and the protective shroud.

Colloid particle sizes are generally in the range of 10 to 20 angstroms, depending on the method of measurement (38). The Pd:Sn ratio is in the range of 0.5 to 1.0, depending on the particle size. When a dielectric surface is immersed in a solution of colloidal catalyst, the colloid is adsorbed on the surface. The coverages of Pd and Sn, as a function of exposure time, are shown in Fig. 12.19a (38).[*] Maximum coverage is usually obtained within several minutes.

It is usually necessary to treat the catalyzed dielectric surface with an accelerator whose function is to selectively remove the stabilizing stannous ions, thus exposing the catalytically active Pd nucleus. Typical accelerating agents are HCl, NaOH, and $HBF_4$ (39). Pd and Sn coverage as a function of time in an accelerating solution are shown in Fig. 12.19b (38).[*] The selectivity for tin removal is apparent.

The catalytic activity of the colloid is dependent on the method of preparation and may be verified by electrochemical measurements. Osaka et al. examined several colloidal catalyst preparations by dipping a gold electrode into the various catalyst mixtures and observing the electrochemical anodic stripping peaks in 1.0M HCl (40). The catalyst activity was proportional to the charge passed for the Pd stripping peak, although the results were only qualitative. This behavior was later quantified by employing a glassy carbon electrode, which has significantly lower background currents in this potential region (41). Coulometry data obtained from stripping curves correlated well to data obtained by microprobe.

Alternate electrochemical methods include observation of the hydrogen adsorption/desorption region on catalyzed gold electrodes and comparing them to the response obtained at bulk Pd (42). This region has been well characterized by Pd by cyclic voltammetry. The response for active catalysts resembles bulk Pd, while less active catalysts show little or no structure in the hydrogen region.

Electrochemical measurements have also demonstrated that colloidal Pd/Sn catalysts are intrinsically more active for formaldehyde oxidation than either bulk Pd or Au (42,43). This is attributable to Pd/Sn alloy formation and is in agreement with the previous discussion regarding the enhanced activity of certain alloys.

# PROPERTIES OF ELECTROLESS COPPER DEPOSITS

The properties and grain structure of electroless copper deposits are dependent on the substrate upon which deposition occurs. The grain structure associated with a conducting catalytic substrate differs markedly from that obtained on an
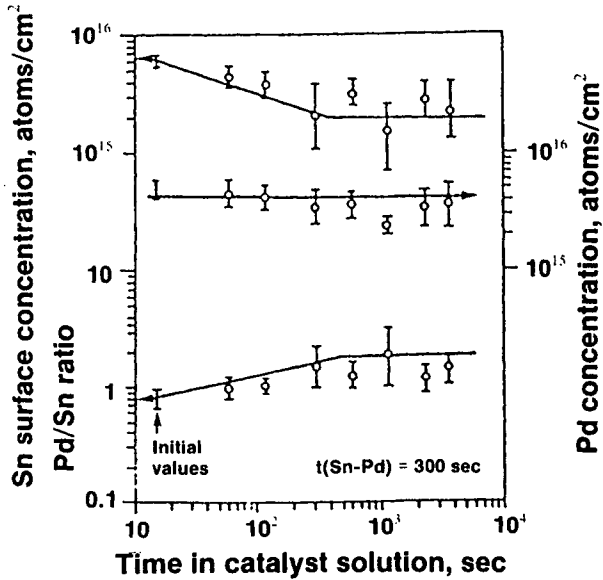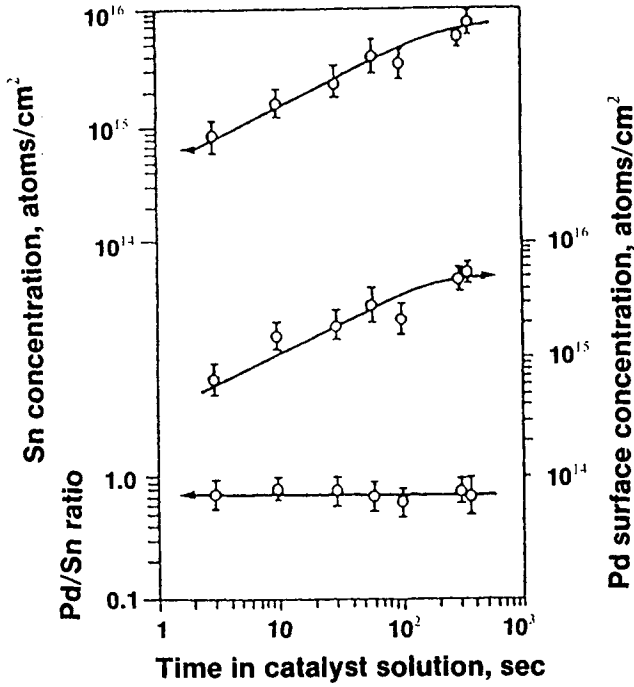
Fig. 12.19—Pd and Sn surface concentration vs. (a) immersion time in S catalyst solution, and (b) accelerator time for an S solution with a catalysis time of 300 sec.

activated or catalyzed nonconductor (44). As an example of the former, electroless deposits on large-grained copper sheets show well defined epitaxial growth. This is in contrast to crystal growth on catalyzed nonconductors, which is of more practical interest and has received the most attention.

Electroless deposits obtained on catalyzed nonconductors generally exhibit fine grain equiaxial growth initially with conversion to larger columnar grains as film thickness increases (Fig. 12.20). Fine grain structure is obtained initially because the catalyst (most frequently colloidal Pd/Sn) is highly dispersed on the nonconducting surface. The catalytic particles, on the dielectric surface, are 10 to 50 nm in diameter and function as discrete centers of nucleation. Notice that there is agglomeration of the particles on the surface since particle sizes measured in solution are approximately an order of magnitude less. During very early stages of exposure in the electroless bath, the grain sizes for copper crystallites at the nonconductor interface are generally observed to be nearly an order of magnitude larger than the catalyst particle agglomerates. Thus, it seems likely that agglomeration of crystallites occurs (45,46). Migration and subsequent agglomeration is possible, since the catalyst particles are not tightly bound to the surface, and probably continues to occur until a complete, uniform film is obtained.

Observation of crystal growth at a catalytic amorphous substrate (e.g., Pd-Cu-Si alloy) exhibits very finely-grained deposits (44). In this case, agglomeration is prevented because the catalytic sites are not mobile and cannot migrate.

In the very early stages of copper deposition on Pd/Sn catalysts, EDAX measurements demonstrate a surface composed primarily of Cu and Pd rather than Cu, Pd, and Sn (47). This may be attributable to the exchange of Cu for Sn, resulting in a solid solution of Cu and Pd. This is supported by the observation that Pd/Sn catalysts are intrinsically more active than Pd. It appears that the galvanic exchange of Sn for Cu is an essential aspect of the catalytic mechanism. Further, the lattice constant observed for the Cu/Pd particles is intermediate between that of Cu and Pd. It therefore seems likely that a solid solution of Cu and Pd is obtained with exclusion of Sn from the lattice.

For formaldehyde-based electroless copper baths, the deposition of copper is accompanied by the liberation of hydrogen, which may cause blistering of the deposit. Inclusion of hydrogen within copper deposits has been verified by the observation of microscopic gas bubbles (44). This phenomena has a direct impact on the physical properties of the deposit. Shown in Table 12.5 (44)** are data from two identical electroless baths, the only difference being the presence of NaCN in bath B. The lower ductility observed for bath A is consistent with the higher occurrence of gas bubbles. The reduction in ductility by incorporated gas bubbles may be attributable to one or both of the following mechanisms: (1) bubbles occurring near grain boundaries serve as fracture sites, thus increasing

## Table 12.5
## Properties of Electroless Copper Deposits*

| | Ductility, % | | | |
| | | | | |
| Bath | As-deposited | After 6 months | Grain size, $\mu$m | Gas bubble density/cm$^3$ |
|---|---|---|---|---|
| A | 1.2 | 4.8 | 0.5 to 1.0 | $9 \times 10^{15}$ |
| B | 3.6 | 4.8 | 0.5 to 1.0 | $9 \times 10^{14}$ |

*Plexiglass substrate.

the possibility of fracturing; (2) finely dispersed bubbles may act as obstacles to the passage of slip dislocations, resulting in increased hardness for the deposit.

It is interesting to note that the ductility for each bath composition improved with time. This may be attributed to the diffusion of hydrogen out of the copper. The diffusivity of hydrogen through copper occurs via an interstitial mechanism and is quite high, although it is impeded to some extent by the presence of voids left by the gas bubbles. This hypothesis is supported by the fact that annealing improves deposit ductility, presumably by accelerating the hydrogen diffusion process (48).

In general, ductility in the range of 4 to 7 percent elongation and tensile strength in the range of 30,000 to 80,000 psi are characteristic of crack-free copper deposits (49). The ductility of electroless copper deposits improves with increasing plating temperatures and decreases with increased plating rate at a given temperature. The tensile strength increases with decreasing plating rate (48). It is clear that lower plating rates tend to yield more favorable metallurgy. However, there continues to be a substantial effort to increase plating rates without sacrificing deposit metallurgy. This may be accomplished, to some extent, by increasing the bath temperature, although bath stability is an issue. One novel approach is to operate the bath at elevated temperatures in a closed system, which results in an increase in pressure (50). The result is an increased plating rate, compared to ambient pressure, with no sacrifice in physical properties.

There are numerous reports, primarily in the patent literature, on the influence of additives on the physical properties of electroless copper deposits (51-52). Additives include cyanide or related nitrile compounds, organo-sulfur compounds, silanes, and surfactants such as polyethylene glycol. Cyanide, as
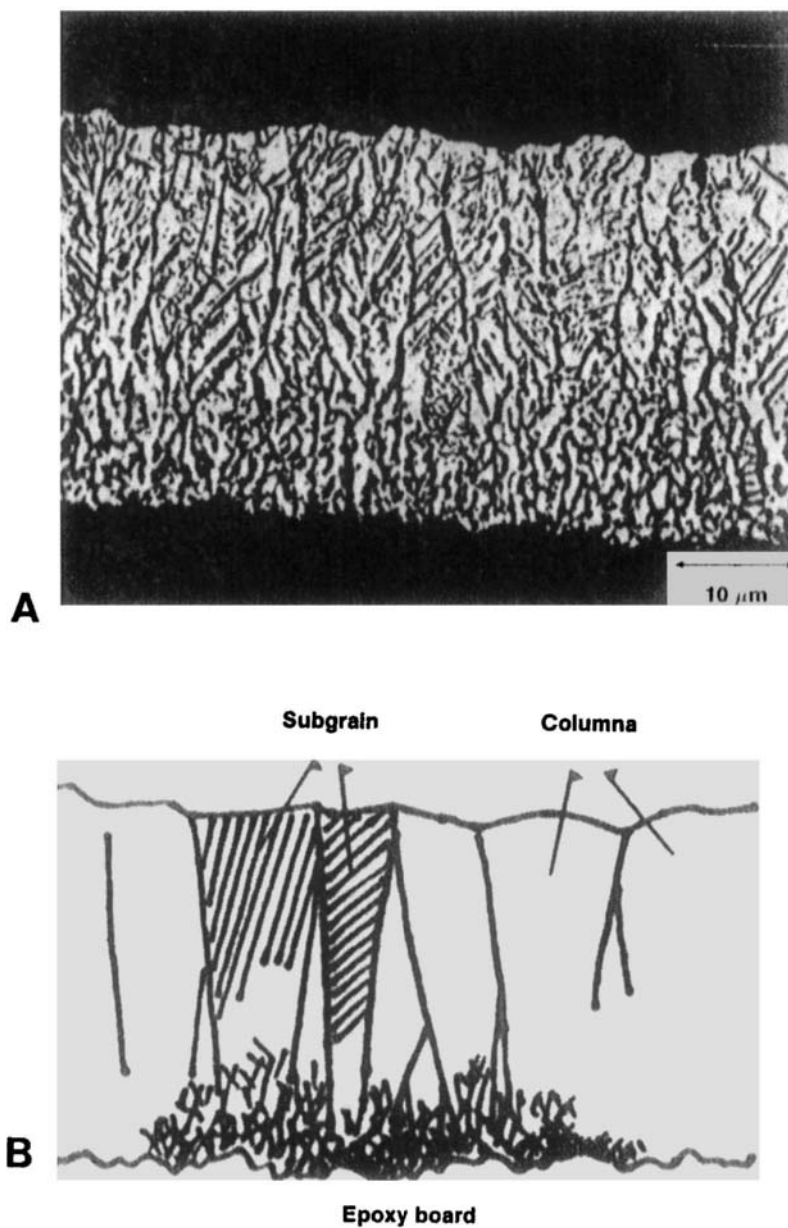
10 μm

A

Subgrain          Columna

B

Epoxy board

Fig. 12.20—Optical micrograph showing cross-section of thick deposit.

illustrated above, not only stabilizes the plating bath but enhances deposit ductility. The mechanism is likely to be that of competitive adsorption of the strongly adsorbed $CN^-$ ion and the intermediate adsorbed hydrogen radical, thus precluding hydrogen entrapment and embrittlement. Addition of polyethylene glycol to electroless copper baths generally improves ductility, particularly at higher molecular weights (53). The mechanism for this and other surfactants is lowering of the overall plating rate compared to an additive-free bath.

Glycine has been observed to decrease the plating rate and increase ductility and tensile strength for copper deposits, although the proposed mechanism is somewhat different than described above (54). Glycine and formaldehyde form a condensation product according to the following reversible equilibrium:

$$NH_2CH_2COOH + HCHO \rightleftharpoons H_2C = NCH_2COOH + H_2O \qquad [41]$$
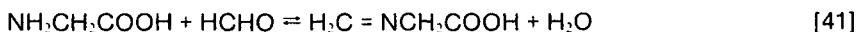
Therefore, increasing the glycine concentration tends to lower the free formaldehyde concentration, which in turn reduces the plating rate and improves the deposit metallurgy. In addition to the above homogeneous reaction, glycine is also a complexant for cuprous ion and may function as a stabilizer in much the same fashion as $CN^-$, although the stability constant is lower for the glycine complex.

Small quantities of metal ions present in the plating solution may also alter the deposit properties. For example, $Ni^{2+}$ ions present in the plating solution have been reported to increase tensile strength and resistivity, but did not alter the ductility (55). Analyzed copper films showed the presence of 0.1 to 1.2 percent nickel incorporated into the deposit. Incorporation of foreign metals in the deposit may not only alter the physical properties, but may also result in a surface with enhanced catalytic activity.

---

# REFERENCES

1. M. Pourbaix, *Atlas of Electrochemical Equilibria*, Pergamon Press, London, 1966.
2. C. Wagner and W. Traud, *Z. Electrochim.*, **44,** 391 (1938).
3. J.V. Petrocelli, *J. Electrochem. Soc.*, **97,** 10 (1950).
4. E.J. Kelly, ibid., **112,** 124 (1965).
5. M. Paunovic, *Plating*, **51,** 1161 (1968).
6. S.M. El-Raghy and A.A. Aho-Solama, *J. Electrochem. Soc.*, **126,** 171 (1979).
7. F.M. Donahue and C.U. Yu, *Electrochem. Acta*, **15,** 237 (1970).
8. A. Molenaar, M.F.E. Holsrinet and L.K.H. van Beek, *Plating*, **61,** 238 (1974).

9. F.M. Donahue and F.L. Shippey, *Plating,* **60,** 135 (1973).
10. F.M. Donahue, *J. Electrochem. Soc.,* **119,** 72 (1972).
11. T.N. Andersen, M.H. Ghandehari and M. Ejuning, ibid., **122,** 1580 (1975).
12. P. Bindra and J. Tweedie, ibid., **130,** 1112 (1983).
13. F.M. Donahue, ibid., **127,** 51 (1980).
14. V.G. Levich, *Physicochemical Hydrodynamics,* Prentice-Hall, Englewood Cliffs, NJ, 1962.
15. A.C. Riddiford, *Advances in Electrochemistry and Electrochemical Engineering,* Vol. 4, Interscience Press, New York, 1966.
16. A.C. Makrides, *J. Electrochem. Soc.,* **107,** 869 (1960).
17. K.J. Vetter, *Electrochemical Kinetics,* Academic Press, New York, 1967.
18. D. Barnes and P. Zuman, *J. Electroanal. Chem.,* **46,** 323 (1973).
19. D. Manousek and J. Volke, ibid., **43,** 365 (1973).
20. W. Vielstich, *Fuel Cells,* D.J.G. Ives translator, Wiley-Interscience Publishers, London, 1970.
21. R.M. Lukes, *Plating,* **51,** 1066 (1964).
22. F.M. Donahue, K.L.M. Wong and R. Bhalla, *J. Electrochem. Soc.,* **127,** 2340 (1980).
23. J. Dumesic, J.A. Koutsky and T.W. Chapman, ibid., **121,** 1405 (1974).
24. R. Schumacher, O.R. Melroy and J.J. Pesek, *J. Phys. Chem.,* **89,** 4338 (1985).
25. D. Vitkavage and M. Paunovic, *Plating,* **70,** 48 (1983).
26. L.N. Schoenberg, *J. Electrochem. Soc.,* **118,** 1521 (1971).
27. J. Ohno, O. Wakabayashi and S. Haruyama, ibid., **132,** 2323 (1985).
28. P. Bindra and J. Roldan, ibid., **132,** 2581 (1985).
29. M. Enyo, *J. Electroanal. Chem.,* **186,** 155 (1985).
30. M. Beltowska-Brzezinksa and J. Heitbaum, ibid., **183,** 167 (1985).
31. M. Enyo, ibid., **201,** 47 (1986).
32. See for example N. Feldstein and J.A. Weiner, *J. Electrochem. Soc.,* **120,** 475 (1973), and references therein.
33. R.J. Zeblisky, U.S. patent 3,672,938.
34. C.R. Shipley, U.S. patent 3,011,920.
35. E.D. D'Ottavio, U.S. patent 3,532,518.
36. R.L. Cohen and K.W. West, *J. Electrochem. Soc.,* **120,** 502 (1973).
37. R.L. Cohen and K.W. West, *Chem. Phys. Lett.,* **16,** 128 (1972).
38. R.L. Meek, *J. Electrochem. Soc.,* **122,** 1177 (1975).
39. R.L. Cohen and R.L. Meek, *Plating and Surf. Fin.,* **63,** 47 (Jun. 1976).
40. T. Osaka, H. Takematsu and K. Nihei, *J. Electrochem. Soc.,* **127,** 1021 (1980).
41. E.J.M. O'Sullivan, J. Horkans, J. White and J. Roldan, *IBM Journal of Research and Dev.,* **32,** 591 (1988).
42. J. Horkans, *J. Electrochem. Soc.,* **130,** 311 (1983).
43. J. Horkans, ibid., **131,** 1853 (1984).
44. S. Nakahara and Y. Okinaka, *Acta Metall.,* **31,** 713 (1983).
45. R. Sard, *J. Electrochem. Soc.,* **117,** 864 (1970).
46. A. Rantell, *Trans. Inst. Metal Finish.,* **48,** 191 (1970).
47. J. Kim et al., *IBM J. of Res. Develop.,* **28,** 697 (1984).

48. J.J. Grunwald, H. Rhodenizer and L. Slominski, *Plating,* **58,** 1004 (1971).
49. M. Paunovic and R. Zeblisky, ibid., **72,** 52 (1985).
50. S.K. Doss and P. Phipps, U.S. patent 4,594,273.
51. O.B. Dutkewych, U.S. patent 3,475,186.
52. F.W. Schneble et al., U.S. patents 3,310,430 and 3,257,215.
53. C.J.G.F. Janssen, H. Jonker and A. Molenaar, *Plating,* **58,** 42 (1971).
54. S. Mizumoto et al., ibid., **73,** 48 (1986).
55. M.L. Khasin and G.A. Kiteau, *J. Appl. Chem. USSR,* **57,** 1971 (1984).
56. F.L. Shippey and F.M. Donahue, *Plating,* **60,** 43 (1973).

# GLOSSARY

| | |
|---|---|
| $A$ | Electrode area |
| $a$ | Tafel slope intercept |
| $B_M$ | Diffusion parameter for [CuEDTA]$^{2-}$ complex |
| $B_{O_2}$ | Diffusion parameter for dissolved oxygen |
| $B_R$ | Diffusion parameter for HCHO |
| $b_M$ | Tafel slope for cathodic partial reaction |
| $b_R$ | Tafel slope for anodic partial reaction |
| $C_M$ | Bulk concentration of copper ions |
| $C_{O_2}$ | Bulk concentration of dissolved oxygen |
| $C_R^s$ | Surface concentration of HCHO |
| $C_R$ | Bulk concentration of HCHO |
| $D_R$ | Diffusion coefficient of HCHO |
| $E$ | Electrode potential |
| $E_v$ | Thermodynamic reversible potential for the metal deposition reaction |
| $E_M^o$ | Standard electropotential for copper deposition |
| $E_{MP}$ | Mixed potential |
| $E_R$ | Thermodynamic reversible potential for reducing agent reaction |
| $E_R^o$ | Standard electropotential for HCHO |
| $F$ | Faraday constant |
| $i_M$ | Current density for metal deposition |
| $i_M^t$ | Total cathodic current density |
| $i_M^k$ | Kinetic controlled current density for metal deposition |
| $i_M^o$ | Exchange current density for metal deposition |
| $i_M^D$ | Diffusion-limited current density for metal deposition |
| $i_M^{D'}$ | Diffusion-limited current density for total cathodic reactions |
| $i_{O_2}$ | Current density for oxygen reduction |
| $i_{plating}$ | Plating current density |
| $i_R$ | Current density for HCHO oxidation |
| $i_R^o$ | Exchange current density for HCHO oxidation |
| $i_R^D$ | Diffusion-limited current density for HCHO oxidation |
| $n_M$ | Number of electrons transferred in metal deposition reaction |
| $n_R$ | Number of electrons transferred in the HCHO oxidation reaction |
| $R$ | Gas constant |
| $T$ | Absolute temperature |
| $v$ | Stoichiometric number |
| $\alpha_M$ | Transfer coefficient for metal deposition |
| $\alpha_R$ | Transfer coefficient for HCHO oxidation reaction |
| $\beta_M$ | Symmetry factor |
| $\gamma$ | Number of preceding steps prior to rds |
| $\eta_M$ | Overpotential for metal deposition |
| $\eta_R$ | Overpotential for HCHO oxidation reaction |
| $\nu$ | Kinematic viscosity |
| $\omega$ | Rotation rate of rotating disk electrode |